Applied Physics Letters ARTICLE scitation.org/journal/apl

Susceptibility of multipactor discharges near a dielectric driven by a Gaussian-type transverse rf electric field

Cite as: Appl. Phys. Lett. **121**, 164103 (2022); doi: 10.1063/5.0121907
Submitted: 20 August 2022 · Accepted: 24 September 2022 ·
Published Online: 21 October 2022

De-Qi Wen,[1,2,a)] Asif Iqbal,[1] Peng Zhang,[1] and John P. Verboncoeur[1,2]

AFFILIATIONS

[1]Department of Electrical and Computer Engineering, Michigan State University, East Lansing, Michigan 48824, USA
[2]Department of Computational Mathematics, Science and Engineering, Michigan State University, East Lansing, Michigan 48824, USA

[a)]Author to whom correspondence should be addressed: wendeqi@msu.edu

ABSTRACT

Multipactor discharge near an rf window is a key limiting factor in high power microwave systems. In this work, we report special features of dielectric multipactor susceptibility under a Gaussian-type waveform as a function of the rf power density of the transverse rf electric field ($\bar{P}_{\mathrm{rf}}$) and normal restoring field (E_{dc}) via particle-in-cell (PIC) and multiple particle Monte Carlo (MC) simulations. The MC simulations show that, for a Gaussian waveform of a half peak width ($\Delta\tau$), larger than $\Delta\tau/T = 0.15$ with $T = 1$ ns the rf repetition period, the susceptibility boundary is similar to that of the conventional sinusoidal waveform-driven multipactor, i.e., two inclined lines in the plane of ($\bar{P}_{\mathrm{rf}}, E_{\mathrm{dc}}$). However, by decreasing $\Delta\tau$, the susceptibility boundary converts to be a closed curve at $\Delta\tau/T = 0.11$ in the plane of ($\bar{P}_{\mathrm{rf}}, E_{\mathrm{dc}}$) and further shrinks at $\Delta\tau/T = 0.05$. PIC simulations with a self-consistent surface and space charge effects also show a reduced E_{dc} with increasing $\bar{P}_{\mathrm{rf}}$ when $\bar{P}_{\mathrm{rf}}$ exceeds a critical value, resulting in a closed curve in the plane of ($\bar{P}_{\mathrm{rf}}, E_{\mathrm{dc}}$), and the maximum time-averaged E_{dc} (multipactor strength) also decreases significantly with further decreasing $\Delta\tau$ in agreement with MC simulations. Accordingly, the fraction of the rf power density absorbed by the multipactor discharges also decreases nonlinearly with $\Delta\tau$ from the order of 10^{-2} to 10^{-3} (even 10^{-4}), implying a significant improvement compared to the conventional sinusoidal waveform. The simulations also show that the multipactor susceptibility under a transverse Gaussian-type waveform for different frequencies follows the same scaling law in terms of the ratio of the electric field to the rf repetition rate.

Multipactor is a nonlinear discharge phenomenon due to electron avalanche near a dielectric surface (rf window) or within a metallic gap in which seed electrons strike the surface repeatedly and induce secondary electron yield (SEY) above unity.[1,2] Multipactor is frequently observed in a multitude of devices such as high-power microwave (HPM) sources, space-based communication systems, rf accelerators, and high voltage insulators from DC to microwaves.[3–6]

Multipactor discharge near a rf window can absorb energy and deposit it to the surface, leading to thermal or stress failure,[7,8] or evaporated gas desorption from the surface. Eventually, a plasma ionization breakdown may occur and cut off the signal transmission.[9–17] Therefore, it is of great importance to suppress single-surface multipactor in order to improve the breakdown threshold and device performance. Historically, TiN coatings on the window were initially adopted to decrease the secondary electron yield (SEY) of the window itself.[18,19] Later, modifying the window geometry, such as periodic grooves on the window surface in rectangular or triangular shape, was shown to reduce multipactor by altering the impact angle of electrons to decrease the electron energy and the flight time.[20–26] In addition, an external dc electric field or a dc magnetic field parallel to the rf window and normal to the transverse electric field is also used to decrease the effective average SEY below unity.[27–29] These methods involve special materials or require the modification of the existing structure of microwave devices, and sometimes make the system unacceptably heavy,[34] especially for space-based satellite communication systems.

In our recent work,[37] a Gaussian-type transverse rf electric field near the rf window was found to have a capability to significantly reduce the multipactor strength via adjusting the half peak width of the Gaussian waveform ($\Delta\tau$) while keeping the transmission power constant. Meanwhile, the Gaussian-type waveform is found to be well

reproduced by adding four higher harmonic components to the fundamental frequency signal.

The multipactor susceptibility diagram is a useful design guidance in practice for workers to make an immediate assessment of the range of rf power and/or electric field strength over which multipactor may occur.[3,30–32] The first susceptibility diagram in the plane of the transverse rf electric field amplitude (E_{rf0}) and restoring field (E_{dc}) was created for the rf electric field parallel to the surface by Kishek *et al.*[3] and extensively investigated for more complicated configurations, such as oblique rf electric fields,[29,33] as well as in the presence of the magnetic field.[33,34] Recently, multi-tone signals also attract interest as they may have potential to break the resonant condition of multipactor in a waveguide[36–38] and result in suppression.[18,20,37,39–43] The susceptibility diagram investigated in the literature focusing on a sinusoidal transverse electric field is mainly characterized by two inclined lines in terms of (E_{rf0}, E_{dc}) corresponding to the first and second crossover energy of the SEY for a given surface material.

In this work, we investigate the susceptibility of multipactor under Gaussian-type transverse electric fields and report its special feature, which significantly differs from the conventional sinusoidal drive and shows favorable effects on signal transmission in high power microwave sources. Here, in order to consider the waveform shape effect, we show the susceptibility diagram in terms of the input rf power ($\bar{P}_{rf}$) and restoring field (E_{dc}). It is found that in the plane of ($\bar{P}_{rf}, E_{dc}$) the susceptibility boundary representing the unit SEY, i.e., the boundary between growth and decay converts to a closed curve and further shrinks when adjusting the half peak width of the Gaussian-type waveform, $\Delta\tau$, from 0.15 to 0.05 T with $T = 1$ ns the rf repetition period. Meanwhile, the fraction of rf power consumed by multipactor discharges is decreased to the order of 10^{-3} (even close to 10^{-4}), significantly lower than that of the sinusoidal waveform (on the order of 10^{-2}).

The multipactor discharge investigated in this work is on the vacuum side of a rf window, and the other side is semi-infinite, as shown in Fig. 1(a). The main simulation tools are particle-in-cell (PIC)[35,37,44,45] and multiple-particle Monte Carlo (MC) simulation.[36] In PIC simulations, the seed electrons and the electron-induced secondary electrons are tracked by thousands of super particles,[29,35,37] in which both surface and space charge effects are incorporated self-consistently. In the MC simulations, around two hundred macroparticles were traced, and the charge and mass of the macroparticle are updated based on the SEY for each impact of the macroparticle on the surface.[36] The SEY for each incident primary electron is treated by Vaughan's empirical model,[46] and the emitted electron velocity satisfies the Maxwell–Boltzmann distribution.[3] The rf window is considered to be silicon dioxide and has a dull surface with smoothness factor $k_s = 1$, and the maximum SEY, around $\delta_{max0} = 2.0$ at normal incidence at the maximum impact energy $E_{max0} = 400$ eV is utilized.

The Gaussian-type waveform shown in Fig. 1(b) has the following form within one repetition period:[37]

$$E_y(t) = E_{rf0}\{\exp[-\beta(t-t_1)^2] - \exp[-\beta(t-t_2)^2]\}, \quad (1)$$

where E_{rf0} is the amplitude and $t_1 = 0.25$ and $t_2 = 0.75$ T are the time instant for the maximum and minimum values of the electric field, respectively. β is a function of $\Delta\tau$, satisfying $\Delta\tau = 2\sqrt{\ln 2/\beta}$. Obviously, the waveform is characterized by the half peak width $\Delta\tau$, and smaller $\Delta\tau$ gives a sharper shape. The corresponding rf power density averaged over one rf period is $\bar{P}_{rf} = c\epsilon_0 \int_0^T E_y^2(t)\mathrm{d}t/T$ with c being the speed of light and ϵ_0 being the permittivity in vacuum.

Figures 2(a)–2(d) show the multipactor susceptibility diagram from MC simulations for conventional sinusoidal and Gaussian-type waveform for various $\Delta\tau/T$ from 0.15 to 0.05, respectively. We can see that the susceptibility at a large $\Delta\tau$ is very similar to the common sinusoidal case[3,38] in the plane of ($\bar{P}_{rf}, E_{dc}$), and the curves for the unit SEY in the susceptibility diagram are two inclined lines, between which the SEY is above the unity and multipactor eventually develops. The lower and upper boundaries correspond to the first and second crossover energy of the SEY curve for the given material. As the hop time of electrons will decrease with increasing E_{dc}, therefore, larger $\bar{P}_{rf}$ (also stronger E_{rf0}) is needed to guarantee that the electrons extract the same averaged energy near the first crossover energy value, and $\sqrt{\bar{P}_{rf}}$ almost linearly increases with increasing E_{dc}.[3] Decreasing the $\Delta\tau/T$ to 0.11, the susceptibility boundaries showing the unit SEY convert to be closed, implying that a considerable region in the plane of ($\bar{P}_{rf}, E_{dc}$) appears where no multipactor will occur. Further decreasing $\Delta\tau/T$ to 0.05, the closed region further shrinks. In the previous work,[37] it was found that for a Gaussian-type transverse electric field, a higher fraction of electrons incident on surface have energy below the first crossover energy of the SEY curve and part of the electrons have energy exceeding the second crossover energy of the SEY curve, leading to a decaying multipactor ultimately for a self-consistently evolving restoring field. These electrons with low or high impact energy are generated by the longer plateau and sharper peak stage, respectively, for the waveform at smaller $\Delta\tau$. For a constant E_{dc}, when the E_{dc} is large enough, the hop time will be shorter. For the emitted secondary electrons within the time phase of the plateau transverse field, the secondary electron emission will be reduced due to the insufficient impact energy (below the first crossover energy). The secondary electrons, emitted when the Gaussian waveform is near the peak value, are capable of extracting energy above the first crossover energy and induce SEY above the unity. Note that no matter whether the impact energy of electrons is between the first and second crossover energy or above the second crossover energy of SEY, these electrons will experience the plateau electric field immediately for the next few rounds of impacts with shorter hop time due to large E_{dc}, giving rise to the SEY below the unity. Therefore, the multipactor is inhibited for a large constant E_{dc} for any $\bar{P}_{rf}$ in the plane of ($\bar{P}_{rf}, E_{dc}$),

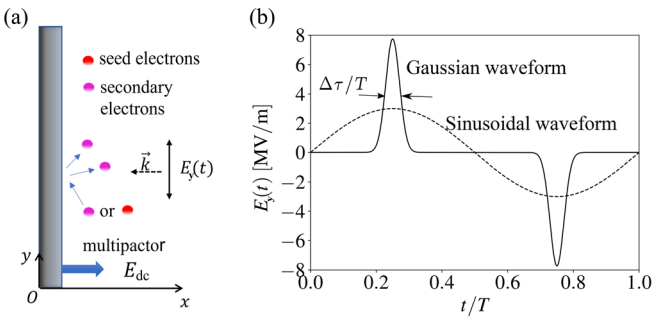

FIG. 1. (a) Diagram of single-surface multipactor discharges near the rf window; (b) the sinusoidal and Gaussian-type transverse rf electric fields for the same input rf power.

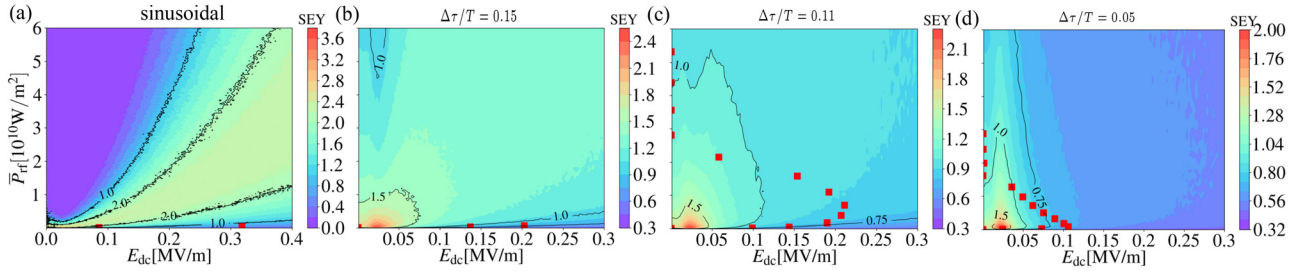

FIG. 2. Multipactor susceptibility for sinusoidal and Gaussian-type transverse rf electric fields, (a) sinusoidal waveform, Gaussian width: (b) $\Delta\tau/T = 0.15$; (c) $\Delta\tau/T = 0.11$; (d) $\Delta\tau/T = 0.05$ in the plane of $\bar{P}_{rf}$ and given constant E_{dc} from multiple-particle Monte Carlo simulation; the red points represent the time-averaged E_{dc} of the time-varying restoring field representing the multipactor strength for various $\bar{P}_{rf}$ from self-consistent PIC simulation.

and the curve of the susceptibility boundary is an enclosed curve for a smaller $\Delta\tau$ of $0.11T$ [see Fig. 2(c)]. The mechanism is more significant for $\Delta\tau/T = 0.05$ that have longer time duration of a plateau transverse electric field, and the corresponding enclosed susceptibility region further shrinks in Fig. 2(d).

PIC simulation can incorporate the self-consistent surface and space charge effect to capture the evolving restoring electric field on the dielectric over time. The time-averaged E_{dc} over a rf period on the surface characterizes the multipactor strength, which is shown by the red points also for the sinusoidal case and $\Delta\tau/T = 0.15, 0.11, 0.05$. Similarly, the $\bar{P}_{rf}$ increases proportionally vs E_{dc} for the sinusoidal case and $\Delta\tau/T = 0.15$. Even though the self-consistently evolving E_{dc} and space charge shielding of outer electrons may allow larger hop time for electrons emitted when the transverse electric field is near the peak, we can see that the PIC simulations still show an enclosed curve in the plane of $(\bar{P}_{rf}, E_{dc})$ for $\Delta\tau/T = 0.11$, i.e., the E_{dc} increases first and starts to decease when $\bar{P}_{rf}$ exceeds some certain values. This applies to the case with smaller $\Delta\tau/T$. The PIC simulations incorporating more physics at the cost of more computation time agree qualitatively with the Monte Carlo simulation in Figs. 2(a)–2(d).

While the restoring field E_{dc} evolves over time self-consistently for the Gaussian-type waveform, the multipactor oscillates accordingly. The oscillating amplitude is measured by PIC simulation and extracted from the time-dependent restoring field as shown in Figs. 3(a)–3(d). The maximum and minimum amplitudes for a given $\bar{P}_{rf}$ are indicated in the range of interest for E_{dc} by the dotted blue line and red line, respectively, which are separated by the black arrow. The oscillating amplitude is gradually getting smaller with decreasing $\Delta\tau/T$ from 0.15 to 0.05. The reason is as follows: for a given $\bar{P}_{rf}$, smaller $\Delta\tau$ means a higher fraction of electrons have energy below the first crossover energy or/and above the second crossover energy, and the effective SEY is decreased, giving rise to a lower growth rate and shorter effective time duration for multipactor development. Therefore, smaller oscillation is produced.

As discussed above, the multipactor discharge can extract energy from the rf electric field, deposit the energy on the surface, and possibly cause thermal or stress failure to the rf window. Ang *et al.*[7] theoretically estimated that the fraction of rf power consumed by multipactor discharge is on the order of 10^{-2}, and thus, it provides reasonable energy for the required heat needed to cause thermal or stress failure of the rf window in experiments by Rimmer.[8] Here, we also explore the fraction of rf power loss due to multipactor by PIC simulations, and the ratio of the temporal multipactor-consumed power density $P_m(t)$ and time-averaged rf power density $\bar{P}_{rf}$, $P_m(t)/\bar{P}_{rf}$ is shown as a function of time t/T in Figs. 3(e)–3(h) for various $\bar{P}_{rf}$. The line plots for three typical $\bar{P}_{rf}$ (also E_{rf0}) are given in Figs. 3(i)–3(l), accordingly. $P_m(t)$ is calculated by collecting the impact energy of individual impact events and integrating over all the incident electrons for one time step at time t. $P_m(t)$ is averaged over 50 time steps to eliminate the statistic noise due to the discrete particles. For a conventional sinusoidal waveform [see Figs. 3(e) and 3(i)], the peak of power ratio $P_m(t)/\bar{P}_{rf}$ occurs near $t/T \approx 0.4$ for a small $\bar{P}_{rf}$. The time moment for the peak value moves ahead and approaches $t/T = 0.25$ when the rf power (transverse electric fields) increases. This is because for smaller $\bar{P}_{rf}$ the induced restoring field E_{dc} is small, which allows for a longer electron hop time, leading to a larger time delay for the maximum $P_m(t)/\bar{P}_{rf}$, which is expected to follow the maximum electric field. A similar trend is also observed for Gaussian-type waveforms $\Delta\tau/T = 0.15$ [see Figs. 3(f) and 3(j)]. The difference is that the instantaneous peak power consumption is higher for $\Delta\tau/T = 0.15$ compared to the sinusoidal case for a strong $\bar{P}_{rf}$ up to 5×10^{10} W/m^2 or higher due to the sharp shape of the waveform. With decreasing $\Delta\tau/T$ to 0.11 and 0.05, the electron hop time is further increased, and the time delay is larger for the occurrence of the peaked $P_m(t)/\bar{P}_{rf}$. The maximum power ratio is also significantly reduced for $\Delta\tau/T = 0.05$. In Fig. 4, we show the time-averaged power ratio $\bar{P}_m/\bar{P}_{rf}$, and we can see that the fraction of rf power consumed by multipactor discharges decreases monotonously from a few percent to the order of 10^{-3} (even 10^{-4}) when the waveform shape is adjusted from a conventional sinusoidal function to a narrower Gaussian-type waveform. Note that the power ratio for $\bar{P}_{rf}$ above 3×10^{10} W/m^2 for $\Delta\tau/T = 0.05$ is not shown in Fig. 4 as the power ratio is almost zero and multipactor cannot be sustained at a saturated state. Similarly, the multipactor cannot be sustained when the $\bar{P}_{rf}$ is large enough [also see Figs. 3(b)–3(d)] for $\Delta\tau/T = 0.15, 0.11$, and the power ratio is almost zero, too.

In addition, we also confirmed the scaling law for Gaussian-type waveforms in terms of E_{rf0} and E_{dc} divided by the rf repetition rate (also known as frequency for the conventional sinusoidal signal) for multipactor driven by different frequencies. Figure 5(a) shows the time-averaged E_{dc} vs various E_{rf0} for a rf repetition rate (f) of 10 and 1 GHz at $\Delta\tau/T = 0.05$ from PIC simulations, and the plots normalized by the rf repetition rate are shown in Fig. 5(b). One can see that E_{dc} keeps increasing in a large range of E_{rf0} compared to the case at 1 GHz. However, after normalizing the plot and comparing the case at 10 GHz to that at 1 GHz, i.e., the red symbols, we can see that the two curves are almost overlapped, similar to the conventional sinusoidal waveform in the literature.[1] Furthermore, the scaling law $(E_{rf0,dc}/f)$ of

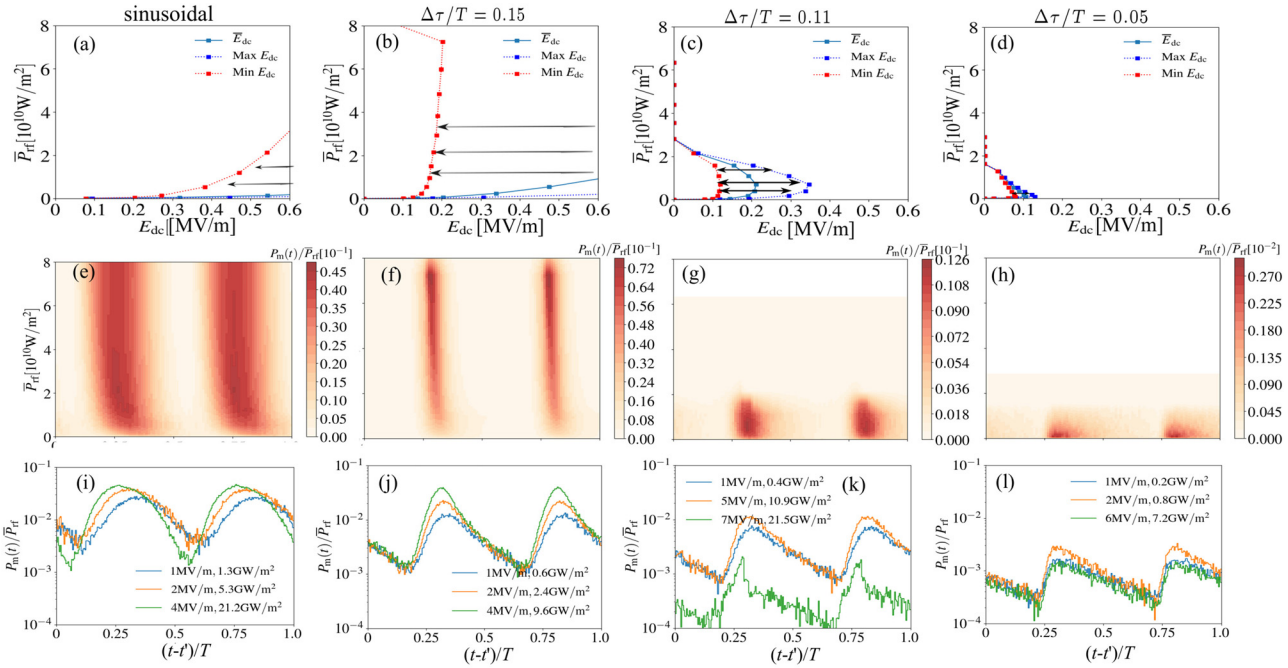

FIG. 3. The maximum, minimum, and the time-averaged value of the restoring field E_{dc} as a function of $\bar{P}_{rf}$ with the black arrow showing the oscillating amplitudes. (a) Sinusoidal waveform, (b) $\Delta\tau = 0.15T$, (c) $\Delta\tau = 0.11T$, and (d) $\Delta\tau = 0.05T$; the corresponding ratio of time-dependent multipactor power consumption, $P_m(t)$, and the time-averaged microwave power, $\bar{P}_{rf}$, (e)–(h); the corresponding line plots for various given rf power, $\bar{P}_{rf}$, also the corresponding transverse electric field amplitude E_{rf0}, (i)–(l), respectively. In (i)–(l), t' equals to nT with n being an integer and represents the time when the multipactor gets saturation after experiencing multipactor development.

the susceptibility diagrams for Figs. 2(a)–2(d) is also examined by MC simulations at 10 GHz, and again the curves are overlapped (not shown here), implying that the physics obtained for 1 GHz may also be valid for different frequencies at least for the range of 1–10 GHz examined, which is expected to be applicable in realistic systems.

In summary, we studied the susceptibility of single-surface multipactor discharges driven by the Gaussian-type transverse electric field.

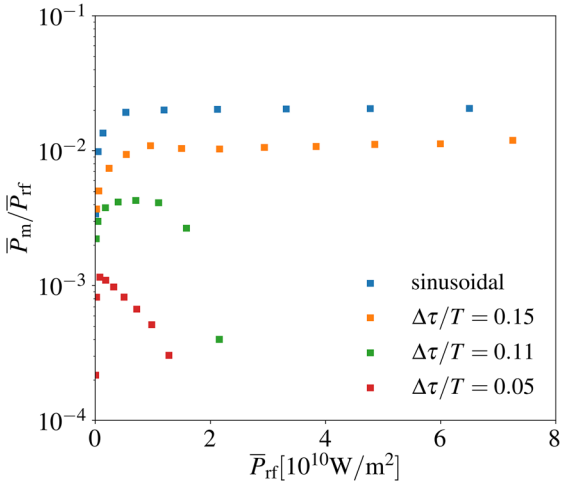

FIG. 4. The time-averaged multipactor and rf power ratio $\bar{P}_m/\bar{P}_{rf}$ as a function of $\bar{P}_{rf}$ for sinusoidal and Gaussian waveforms with different $\Delta\tau$.

Different from conventional sinusoidal waveform-driven multipactor discharges, where the susceptibility boundaries consist of two inclined lines, i.e., the rf power density $\bar{P}_{rf}$ or transverse electric field E_{rf0} increases with increasing restoring field E_{dc} in the plane of $(\bar{P}_{rf}, E_{dc})$, MC simulations indicate the susceptibility boundary converts to a closed curve in terms of $(\bar{P}_{rf}, E_{dc})$, and the region shrinks when decreasing the half peak width of the Gaussian-type waveform from 15% to 5% of the rf repetition period. PIC simulation also confirmed that the time-averaged E_{dc} increases first and then decreases when increasing the rf power density or transverse electric field magnitude, in agreement with the MC simulations for Gaussian-type waveforms with different half peak widths. Meanwhile, the fraction of the rf power density consumed by multipactor discharges decreases from the order of 10^{-2} for a conventional sinusoidal waveform to the order of 10^{-3} (even 10^{-4}) for a Gaussian-type waveform with half peak width 5% of the rf repetition period. This results in an increasing power threshold for breakdown in high power microwave devices and avoidance of rf window failure. Finally, the scaling law of the susceptibility diagram in the plane of (E_{rf0}, E_{dc}) is also examined by normalizing the results to the rf repetition rate. The relationship between E_{rf0} and E_{dc} is found to be the same at 1 and 10 GHz, implying the preferable properties of multipactor susceptibility under Gaussian-type waveform may be applied in a wide range of frequencies in realistic applications of high-power microwave sources.

This work was supported by the Air Force of Scientific Research (AFOSR) MURI under Grant Nos. FA9550-18-1-0062 and FA9550-21-1-0367.

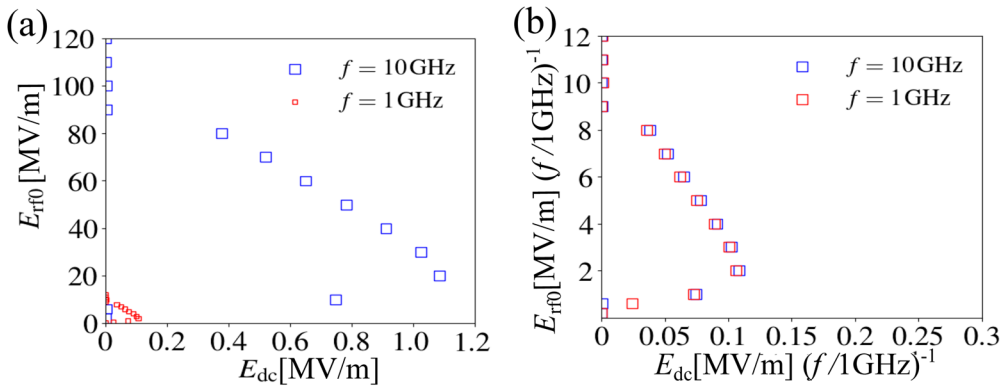

FIG. 5. The time-averaged restoring field E_{dc} vs various E_{rf0} at 10 and 1 GHz, respectively, for $\Delta\tau/T = 0.05$ (a) and its normalization to repetition rate (b).

AUTHOR DECLARATIONS

Conflict of Interest

The authors have no conflicts to disclose.

Author Contributions

De-Qi Wen: Conceptualization (lead); Data curation (equal); Formal analysis (lead); Investigation (lead); Methodology (equal); Visualization (lead); Writing – original draft (lead). **Asif Iqbal:** Data curation (equal); Formal analysis (equal); Investigation (equal); Methodology (equal); Resources (equal); Visualization (equal); Writing – review & editing (equal). **Peng Zhang:** Formal analysis (equal); Funding acquisition (equal); Investigation (equal); Methodology (equal); Project administration (equal); Resources (equal); Visualization (equal); Writing – review & editing (equal). **John P. Verboncoeur:** Formal analysis (equal); Funding acquisition (equal); Investigation (equal); Methodology (equal); Project administration (equal); Resources (equal); Visualization (equal); Writing – review & editing (equal).

DATA AVAILABILITY

The data that support the findings of this study are available from the corresponding author upon reasonable request.

REFERENCES

[1]R. A. Kishek and Y. Y. Lau, Phys. Rev. Lett. **80**, 193 (1998).
[2]R. A. Kishek and Y. Y. Lau, Phys. Rev. Lett. **75**, 1218 (1995).
[3]R. A. Kishek, Y. Y. Lau, L. K. Ang, A. Valfells, and R. M. Gilgenbach, Phys. Plasmas **5**, 2120 (1998).
[4]J. G. Power, W. Gai, S. H. Gold, A. K. Kinkead, R. Konecny, C. Jing, W. Liu, and Z. Yusof, Phys. Rev. Lett. **92**, 164801 (2004).
[5]R. A. Kishek, Phys. Rev. Lett. **108**, 035003 (2012).
[6]M. T. P. Aldan, Ph.D. thesis, University of California, Berkely, 2015.
[7]L.-K. Ang, Y. Y. Lau, R. A. Kishek, and R. M. Gilgenbach, IEEE Trans. Plasma Sci. **26**, 290 (1998).
[8]R. A. Rimmer, Ph.D. dissertation, University of Lancaster, UK, 1988.
[9]Y. Y. Lau, J. P. Verboncoeur, and H. C. Kim, Appl. Phys. Lett. **89**, 261501 (2006).
[10]C. Chang, M. Zhu, J. Verboncoeur, S. Li, J. Xie, K. Yan, T. Luo, and X. Zhu, Appl. Phys. Lett. **104**, 253504 (2014).
[11]Y. Hidaka, E. M. Choi, I. Mastovsky, M. A. Shapiro, J. R. Sirigiri, and R. J. Temkin, Phys. Rev. Lett. **100**, 035003 (2008).
[12]S. K. Nam and J. P. Verboncoeur, Phys. Rev. Lett. **103**, 055004 (2009).
[13]J.-P. Boeuf, B. Chaudhury, and G. Q. Zhu, Phys. Rev. Lett. **104**, 015002 (2010).
[14]H. C. Kim and J. P. Verboncoeur, Phys. Plasmas **13**, 123506 (2006).
[15]D.-Q. Wen, P. Zhang, J. Krek, Y. Fu, and J. P. Verboncoeur, Appl. Phys. Lett. **119**, 264102 (2021).
[16]D.-Q. Wen, P. Zhang, J. Krek, Y. Fu, and J. P. Verboncoeur, Phys. Rev. Lett. **129**, 045001 (2022).
[17]D.-Q. Wen, P. Zhang, J. Krek, F. Yangyang, and J. P. Verboncoeur, Plasma Sources Sci. Technol. **31**, 095004 (2022).
[18]S. Michizono, Y. Saito, S. Yamaguchi, and S. Anami, IEEE Trans. Electr. Insul. **28**, 692 (1993).
[19]Suharyanto, S. Michizono, Y. Saito, Y. Yamano, and S. Kobayashi, Vacuum **81**, 799 (2007).
[20]A. Neuber, G. F. Edmiston, J. T. Krile, H. Krompholz, J. C. Dickens, and M. Kristiansen, IEEE Trans. Magn. **43**, 496 (2007).
[21]J. M. Sattler, R. A. Coutu, R. Lake, T. Laurvick, T. Back, and S. Fairchild, J. Appl. Phys. **122**, 055304 (2017).
[22]A. Iqbal, J. Ludwick, S. Fairchild, M. Cahay, D. Gortat, M. Sparkes, W. O'Neill, T. C. Back, and P. Zhang, J. Vac. Sci. Technol. B **38**, 013801 (2020).
[23]M. Mirmozafari, A. Iqbal, P. Zhang, N. Behdad, J. H. Booske, and J. P. Verboncoeur, Phys. Plasmas **29**, 082109 (2022).
[24]J. Ludwick, A. Iqbal, D. Gortat, J. D. Cook, M. Cahay, P. Zhang, T. C. Back, S. Fairchild, M. Sparkes, and W. O'Neill, J. Vac. Sci. Technol. B **38**, 054001 (2020).
[25]C. Chang, Y. D. Li, J. V. Y. S. Liu, and C. L. Liu, Phys. Plasmas **24**, 040702 (2017).
[26]C. Chang, H. J. Huang, G. Z. Liu, C. H. Chen, Q. Hou, J. Y. Fang, X. X. Zhu, and Y. P. Zhang, J. Appl. Phys. **105**, 123305 (2009).
[27]P. Oijala and M. Ukkola, Nucl. Instrum. Methods Phys. Res., Sect. A **474**, 197 (2001).
[28]C. Chang, X. Zhu, G. Liu, J. Fang, R. Xiao, C. Chen, H. Shao, J. Li, H. Huang, Q. Zhang *et al.*, Prog. Electromagn. Res. **101**, 157 (2010).
[29]D.-Q. Wen, P. Zhang, Y. Fu, J. Krek, and J. P. Verboncoeur, Phys. Plasmas **26**, 123509 (2019).
[30]A. Valfells, J. P. Verboncoeur, and Y. Y. Lau, IEEE Trans. Plasma Sci. **28**, 529–536 (2000).
[31]H. Wang, D. Liu, L. Liu, M. Xie, and L. Meng, Plasma Sources Sci. Technol. **27**, 125006 (2018).
[32]P. Zhang, Y. Y. Lau, M. Franzi, and R. M. Gilgenbach, Phys. Plasmas **18**, 053508 (2011).
[33]A. Valfells, L. K. Ang, Y. Y. Lau, and R. M. Gilgenbach, Phys. Plasmas **7**, 750 (2000).
[34]C. Chang, J. Verboncoeur, S. Tantawi, and C. Jing, J. Appl. Phys. **110**, 063304 (2011).
[35]H. C. Kim and J. P. Verboncoeur, Phys. Plasmas **12**, 123504 (2005).
[36]A. Iqbal, J. Verboncoeur, and P. Zhang, Phys. Plasmas **26**, 024503 (2019).

[37]D.-Q. Wen, A. Iqbal, P. Zhang, and J. P. Verboncoeur, Phys. Plasmas **26**, 093503 (2019).
[38]A. Iqbal, J. Verboncoeur, and P. Zhang, Phys. Plasmas **25**, 043501 (2018).
[39]J. Foster, M. Thomas, and A. Neuber, J. Appl. Phys. **106**, 063310 (2009).
[40]C. Chang, G. Liu, C. Tang, C. Chen, H. Shao, and W. Huang, Appl. Phys. Lett. **96**, 111502 (2010).
[41]A. Iqbal, P. Y. Wong, D.-Q. Wen, J. P. Verboncoeur, and P. Zhang, IEEE Trans. Plasma Sci. **49**, 3284 (2021).
[42]A. Iqbal, P. Y. Wong, D.-Q. Wen, S. Lin, J. Verboncoeur, and P. Zhang, Phys. Rev. E **102**, 043201 (2020).
[43]A. Iqbal, J. Verboncoeur, and P. Zhang, Phys. Plasmas **29**, 012102 (2022).
[44]D.-Q. Wen, J. Krek, J. T. Gudmundsson, E. Kawamura, M. A. Lieberman, and J. P. Verboncoeur, Plasma Sources Sci. Technol. **30**, 105009 (2021).
[45]D.-Q. Wen, J. Krek, J. T. Gudmundsson, E. Kawamura, M. A. Lieberman, and J. P. Verboncoeur, IEEE Trans. Plasma Sci. **50**, 2548 (2022).
[46]J. R. M. Vaughan, IEEE Trans. Electron Devices **40**, 830 (1993).